Analog Signalling with 'Digital' Molecular Switches

Stephen E. Clarke

Stanford University
Department of Bioengineering
318 Campus Drive, E350B
Stanford, CA
94305
United States of America
stclarke@stanford.edu

Abstract

Molecular switches, such as the protein kinase CaMKII, play a fundamental role in cell signalling by decoding inputs into either high or low states of activity; because the high activation state can be turned on and persist after the input ceases, these switches have earned a reputation as 'digital'. Although this binary perspective has been valuable for understanding synaptic plasticity over long timescales, accumulating experimental evidence suggests that molecular switches also control cellular processing on short timescales. To investigate this idea further, a non-autonomous, nonlinear ordinary differential equation, representative of a bistable molecular switch, is analyzed. The existence and uniqueness of model solutions to arbitrary input is proved for both the high and low states of activity. These results suggest that sub-state switch activity is an analog signal that tracks instantaneous input frequency, thereby increasing the capacity for information transfer to downstream cellular targets. Using simple dynamics based on the ubiquitous Hill equation, the model and theory make intriguing predictions about synaptic plasticity and suggest a multiplexed encoding of instantaneous frequency information over short timescales, with integration of total activity over long timescales, helping to reconcile contrasting perspectives presented in the literature.

Keywords: molecular switches, frequency coding, stochastic resonance, cellular computation, CaMKII, presynaptic plasticity

Introduction

Many different cellular inputs lead to transient changes in cytosolic calcium (Ca^{2+}) levels, generating temporally complex signals that reflect a wealth of information [1]. As such, cells express highly conserved molecular decoders capable of translating Ca^{2+} oscillations into downstream signalling events that affect diverse processes such as gene transcription, development and aging, neural network homeostasis and the synaptic plasticity that underlies learning and memory [2-9]. A celebrated example of a Ca^{2+} decoder is the bistable molecular switch Ca^{2+}/calmodulin (CaM)-dependent protein kinase II (CaMKII; Box 1), which is driven by transient levels of cytosolic Ca^{2+} into either high or low states of activity. When stabilized through negative regulation by phosphatases, self-exciting kinases such as CaMKII are an ideal component of signal amplification and have been previously likened to transistors on a computer chip, in that they may be turned on or off, presenting an ideal substrate for computation in cellular systems [10].

The classic CaMKII experiments of De Koninck and Schulman provided the first demonstration that a molecular switch can decode the frequency of periodic Ca^{2+} pulses into distinct levels of persistent activation [11]. Subsequent modelling of CaMKII autophosphorylation dynamics captured this hysteresis effect, that is, the ability of the high activation state to persist beyond the original Ca^{2+} signal and act enzymatically over long timescales [12-14]. In these studies, the relationship between Ca^{2+} concentration and the state of the molecular switch was determined from simulations of large, parameterized systems of differential equations that are not readily amenable to deeper mathematical analysis; furthermore, these studies were restricted to periodic inputs. One notable exception is the work of Graupner and Brunel, who developed a reduced Ca^{2+} based model of long timescale postsynaptic plasticity [15]. In order to better understand frequency coding over short timescales, this article analyzes a reduced description of molecular switch behaviour when subject to general aperiodic forcing and in the presence of noise. As the study of cellular information processing shifts from

individual transduction pathways, toward the emergent properties of complex signalling networks, simple mathematical models are becoming indispensable tools for both experimentalist and theoreticians alike [16, 17].

Box 1: The bistable molecular switch CaMKII and synaptic plasticity

Accounting for approximately 1-2% of all brain protein, the molecular switch CaMKII is a central hub of cell signalling networks and can exert both pre- and post-synaptic control over information transmission in the central nervous system [18]. Once bound to the Ca^{2+}-CaM complex, the kinase's ability to cooperatively autophosphorylate produces two distinct stable states: either high or low levels of enzymatic activation.

Postsynaptically, after repetitive stimulation, the high activation state may persist long after the calcium signal subsides and can strengthen the connection between neurons, for example, the hippocampal CA3-CA1 synapses that support learning and memory [19]. Presynaptically, CaMKII also modifies connection strength [20-22]. At mouse hippocampal CA3-CA1 synapses, knocking-out the αCaMKII isoform leads to reduced synaptic potentiation under paired pulse facilitation protocols when compared to the wild-type [23]. Through enzymatic phosphorylation of voltage gated Ca^{2+} channels and ryanodine receptors, αCaMKII can enhance Ca^{2+} entry and Ca^{2+}-induced Ca^{2+} release in response to high frequency signals [24]. However, at the same CA3-CA1 synapses, post-tetanic potentiation protocols generate enhanced levels of potentiation in the knock-out mice, illustrating that αCaMKII may also limit neurotransmitter release depending on the frequency and duration of the input [23]. Furthermore, a frequency dependent shift from paired pulse facilitation to paired pulse depression has been reported [25] and αCaMKII has been shown to serve as a negative, activity-dependent regulator of neurotransmitter release probability [26]. This effect can be partially explained by the fact that CaMKII phosphorylates Ca^{2+} -activated potassium channels that hyperpolarize the presynaptic terminal [27], decreasing the likelihood of Ca^{2+} entry and neurotransmitter release. Intriguingly, αCaMKII also plays a non-enzymatic role in presynaptic CA3-CA1 plasticity by regulating the number of docked synaptic vesicles containing neurotransmitter [28]. In this case, decreased transmitter release is likely explained by the fact that αCaMKII is acting as a sink for intracellular Ca^{2+}, lowering the cytosolic levels that drive the machinery of synaptic vesicle fusion and influencing the size of the readily releasable vesicle pool [29, 30].

One of the most influential discoveries about CaMKII is its ability to decode the frequency of periodic Ca^{2+} pulses into distinct amounts of long lasting, autonomously activated kinase [11]. However, the interpretation of CaMKII as a frequency decoder has been criticized based on the fact that mean values of activity, evoked by different combinations of Ca^{2+} pulse size, duration and frequency, are ambiguously mapped into the same level of autonomously activated switch [31]. To address this criticism and bridge our understanding of CaMKII function over short and long timescales, this article investigates whether the concentration of activated switch acts as a reliable, sub-state analog signal that encodes frequency information over short timescales, where Ca^{2+} pulse size and duration are stable [32]. The experimental evidence discussed above suggests that frequency coding by these 'digital' molecular switches is more sophisticated than previously thought and that fluctuations in presynaptic

αCaMKII activity meaningfully decode instantaneous frequency information, translating it into bidirectional, real-time control of synaptic strength.

Results

A Bistable Switch Model The following differential equation is an abstraction of a bistable molecular switch and was originally proposed as a model of genetic development by Lewis et al. [33]. This relatively simple model is a useful analytical tool to understand the general properties of bistable kinetic systems; although the model interpretation and results are centered on CaMKII and synaptic plasticity, the reader is encouraged to consider the broader implications for instantaneous frequency coding with molecular switches (e.g., mitogen-activated protein kinases).

$$\frac{dy}{dt} = k_0 s - k_1 y + \frac{k_2 y^n}{k_3{}^n + y^n}$$

In this formulation, the level of activated CaMKII (y) is stimulated by the presence of Ca^{2+} bound to CaM (s), which will be studied as a function of time. For simplicity we assume that pulses of Ca^{2+} are bound upon cell entry, which is reasonable since CaM is found in large concentrations surrounding Ca^{2+} channels and has a strong affinity for Ca^{2+} [34]. Deactivation is directly proportional to the active CaMKII concentration at a rate k_1, representing the collective activity of protein phosphatases. Finally, once activated, CaMKII has the ability to cooperatively bind Ca^{2+}- CaM and autophosphorylate itself, which motivates the nonlinear, positive feedback term captured by the Hill equation, where k_2 and k_3 are the association and dissociation constants respectively. Due to physiological constrains, $y,\ s,\ k_0,\ k_1,\ k_2,\ k_3 \geq 0$.

This generic model has been previously applied to genetic networks [33, 35, 36], transcriptional regulation [37, 38], mitogen-activated protein kinases [39], and incorporated into a larger

phenomenological model of presynaptic plasticity [40]. Although insightful for their specific systems, these studies retain a large numbers of parameters that clutter analysis and obscure the generality of the results. Therefore, it is desirable to reduce the number of parameters and facilitate the following analysis by performing routine nondimensionalization. Let $y = x \cdot k_3$, $r = \frac{k_1 k_3}{k_2}$, $s = \frac{k_2}{k_0} c$ and $t = \frac{k_3}{k_2} \tau$, which, when substituted into the original equation and simplifying gives the reduced but dynamically equivalent form:

$$\frac{dx}{d\tau} = c - rx + \frac{x^n}{1 + x^n} \qquad (1)$$

This article is interested in a time varying $c \equiv c_0 + c_l(\tau)$, where c_0 reflects residual cytosolic Ca^{2+} whose slow dynamics are treated as fixed on the fast timescales over which the local Ca^{2+} signal $c_l(\tau)$ fluctuates [41]. The scale factor $T = \frac{k_3}{k_2}$, the quotient of the switch deactivation and activation parameters, will be reintroduced later in order to connect the switch dynamics to time in seconds and stimulation frequency in Hz. Finally, for highly cooperative reactions, $n = 2$ is a reasonable approximation [42] and a convention maintained by all of the studies listed above. The following bifurcation analysis is illustrated for $n = 2$, which allows for exact analytical solutions (Fig. 1 and Methods); however, the main results are then generalized to arbitrary $n \in \mathbb{R}^+$, which is much more realistic and has important consequences for frequency coding.

Stability and Bifurcation Analysis

Although interested in frequency-driven fluctuations, we must first examine the fixed state behaviours of the bistable switch. An important reason for reducing the number of model parameters is to simplify the analysis of how the behaviour of the system changes as a function of the parameter values. For Equation 1, having selected $n = 2$, we only need to consider the effect of varying r and c; depending

on their values, we may have one, two or three equilibrium points (x^*), where the rate of change of the switch $f(x) = c - rx + \frac{x^2}{1+x^2}$ is equal to zero. For example, consider the values $r = 0.52$ and $c = 0.04$ that support bistability: there are three fixed points, two of which are stable, as illustrated by the switch's potential function $U(x) = -\int f(x)dx$ (Fig. 1A). As r and c change, saddle node bifurcations can occur, resulting in the presence of only the high or low activation state. The corresponding bifurcation diagrams are displayed in Figure 1B; their derivation is found in the Methods section.

A key feature of bistability is the hysteresis effect, where the same value of a parameter may evoke different states depending on the history of activity. For example, as c increases, x^* grows larger until crossing the rightmost c_c, where a saddle node bifurcation occurs and the switch jumps up to the high activation state as the low state disappears (Fig. 1B, i). Now, as c decreases back into the bistable range, the high activation state is preserved, and only lost when c crosses below the leftmost value of c_c. This history dependent behaviour is presumably central to CaMKII activity and the synaptic plasticity that underlies learning and memory (Box 1) [19]. A similar phenomenon occurs for the negative regulation parameter r (Fig. 1B, ii). The values of r_c and c_c are plotted parametrically as a function of the active switch in the bifurcation curves (Fig 1B, iii). The bifurcation surface summarizes this information completely (Fig. 1B, iv).

Existence of Sub-state Solutions

To date, studies of Lewis et al.'s model have been restricted to static input and periodic forcing. It is of principal interest to characterize the model behaviour in response to aperiodic forcing, in order to gain a more general, physiologically realistic understanding of frequency coding with molecular switches. In

addition to coding frequency information into stable levels of activated switch for minutes to hours [11, 19], what about frequency coding on the order of milliseconds to seconds? In a region surrounding a stable activation state, is there a unique sub-state solution for a time varying input signal? This question is not trivial, since small changes in the initial conditions of a nonlinear system (i.e., past switch activity) may generate drastically different behaviours. Understanding the relationship that determines whether solutions converge or diverge provides valuable insight into the properties of bistable molecular switches.

We now reintroduce the scale factor T since, in the following section, we are interested in studying frequency in Hz and time in seconds (t). As such, Equation 1 becomes

$$T\frac{dx}{dt} = c(t) - rx + \frac{x^n}{1+x^n} \qquad (2)$$

First, to establish the existence of solutions around the high and low switch states, consider Equation 2 and note that f explicitly depends on the time-varying forcing term, $c(t) \equiv c_0 + c_l(t)$. The function $f(t, x(t))$ is assumed to be Lipschitz continuous and well-defined within strips, $y_- \le x(t) \le y_+$ satisfying the conditions $f(t, y_-) > 0$ and $f(t, y_+) < 0 \ \ \forall t \in \mathbb{R}^+$, which trap solutions within these boundaries. For (c, r) corresponding to the bistable region of parameter space (Fig. 1B, iii), there exist two infinite strips, $x(t) \in (y_{l-}, y_{l+})$ and $x(t) \in (y_{h-}, y_{h+})$, each surrounding one of the stable equilibrium points (x^*). Now, we wish to locate values for the low state (y_{l-}, y_{l+}) and high state (y_{h-}, y_{h+}), where the existence of local time-varying solutions can be guaranteed. This problem is intimately linked to bifurcation, since y_{l+} and y_{h-} depend on the values of c and r. The choice of a lower bound for the strip that exists around the low activation state is $y_{l-} = 0$, since the physiological restriction $c(t) \ge 0$ implies $f(t, 0) > 0 \ \ \forall t$, ignoring the degenerate case of $c(t) = x(t) = 0$. The upper

bound of the lower strip, y_{l+}, should occur at a value $x_u^* - \Delta x$, left of the unstable equilibrium where $f(t, x_u^*) = 0$, such that $\Delta c + f(t, x_u^* - \Delta x) < 0, \forall t$; this condition ensures that the system is not trivially displaced into the up-state by a single Ca^{2+} pulse with amplitude Δc. For the high concentration strip (y_{h-}, y_{h+}), the lower bound y_{h-} is chosen as a value of x infinitesimally greater than x_u^*, that is, $y_{h-} = x_u^* + \varepsilon$ for $\varepsilon \to 0$. Since we have restricted r and $c > c_c$ (leftmost) to the bistable range, we know that $f(t, y_{h-}) > 0 \ \ \forall t$. For the upper bound of the high activation strip, it is enough to note that for $x > x_h^*$, $f(t, x(t)) < 0 \ \ \forall t$ and, since we wish to maximize the width of the strip, we take x arbitrarily large, denoting this value by $y_{h+} = x_\infty$. During stimulation, if (c, r) drifts out of the bistable region of parameter space, a saddle node bifurcation occurs and only one infinite strip exists; in this case, $y_- = 0$ and $y_+ = x_\infty$.

By invoking the Cauchy-Peano theorem, we guarantee the existence of at least one sub-state solution for every initial condition found within the strip regions defined above, since the conditions on the sign of the derivative $f(t, x(t))$ define trapping regions. However, this theorem says nothing about whether solutions starting at different initial conditions will converge to a unique, stimulus-driven response and track the instantaneous frequencies of the input signal.

Uniqueness of Sub-state Solutions

As motivation for the following results, Figure 2A shows an example switch response to an 8 Hz Poisson pulse sequence, which is convolved with an alpha function filter (30 ms; Methods), then normalized to the signal's maximum and scaled by $\Delta c = 0.5$ to create a representative input signal, which the switch tracks closely.

We now establish the stability and uniqueness of solutions in each strip for distinct initial conditions. Consider a general infinite strip (y_-, y_+), where $x(t)$ is a solution to Equation 2 with initial condition $x_0 \in (y_-, y_+)$. Assume there is another solution, $u(t)$, with a different initial condition $u_0 \in (y_-, y_+)$. Writing $z(t) = |u(t) - x(t)|$ and first assuming n is a positive integer, we see that

$$
\begin{aligned}
\frac{d}{dt} z(t) &= \lim_{h \to 0} \frac{z(t+h) - z(t)}{h} \\
&= \lim_{h \to 0} \frac{\left|u(t+h) - x(t+h)\right| - \left|u(t) - x(t)\right|}{h} \\
&\le \lim_{h \to 0} \frac{\left|(u(t+h) - x(t+h)) - (u(t) - x(t))\right|}{h} \\
&= \lim_{h \to 0} \frac{\left|(u(t+h) - u(t)) - (x(t+h) - x(t))\right|}{h} \\
&= \operatorname{sgn}[u(t) - x(t)] \cdot \frac{d}{dt}(u(t) - x(t)) \\
&= T^{-1} \operatorname{sgn}[u(t) - x(t)] \left(c(t) - r \cdot u(t) + \frac{u^n(t)}{1 + u^n(t)} - \left(c(t) - r \cdot x(t) + \frac{x^n(t)}{1 + x^n(t)} \right) \right) \\
&= T^{-1} \operatorname{sgn}[u(t) - x(t)] \cdot \left(-r \cdot (u(t) - x(t)) + \frac{u^n(t) - x^n(t)}{(1 + u^n(t))(1 + x^n(t))} \right) \\
&= T^{-1} \operatorname{sgn}[u(t) - x(t)] \cdot (u(t) - x(t)) \cdot \left(-r + \frac{u^n(t) - x^n(t)}{(u(t) - x(t))(1 + u^n(t))(1 + x^n(t))} \right) \\
&= T^{-1} \left|u(t) - x(t)\right| \cdot \left(-r + \frac{\sum_{i=1}^{n} u^{i-1}(t) \cdot x^{n-i}(t)}{(1 + u^n(t))(1 + x^n(t))} \right) \qquad \text{for } n \in Z^+ \\
&= T^{-1} z(t) \cdot \left(-r + p(u, x, n) \right)
\end{aligned}
$$

The expression $p(u, x, n)$ reflects a tendency for solutions to diverge and achieves a maximum at an intermediate switch level that separates the low and high states of activation. Now, consider $p(u, x, n)$ for the special case of $n = 2$, used in the bifurcation analysis; in this case, $p(u, x, 2) = \dfrac{u + x}{(1 + u^2)(1 + x^2)}$, which is plotted in Figure 2B. Setting the partial derivatives of the function to zero and solving for u

and x, yields a critical point: $(u,x)=\left(\frac{\sqrt{3}}{3},\frac{\sqrt{3}}{3}\right)$. Substituting this into p gives a global maximum of $\frac{3\sqrt{3}}{8}$. Since $\frac{d}{dt}z(t)\le T^{-1}\left(-r+\frac{3\sqrt{3}}{8}\right)z(t)\ \ \forall t$, we can apply Grönwall's inequality, which gives us the following:

$$z(t)\le e^{T^{-1}\int_0^t(-r+\frac{3\sqrt{3}}{8})ds}$$

Substituting the expression for $z(t)$ and solving this integral exponent yields,

$$|u(t)-x(t)|\le e^{-T^{-1}(r-\frac{3\sqrt{3}}{8})t}$$

and, as $t\to\infty$, we have

$$0\le\lim_{t\to\infty}|u(t)-x(t)|\le\lim_{t\to\infty}e^{-T^{-1}(r-\frac{3\sqrt{3}}{8})t}$$

For $r>\frac{3\sqrt{3}}{8}$ (≈ 0.65), we obtain

$$0\le\lim_{t\to\infty}|u(t)-x(t)|\le 0$$

By the squeeze theorem we conclude that $|u(t)-x(t)|\to 0$ as $t\to\infty$. Therefore, a unique frequency-driven solution exists within either strip and is independent of the initial conditions. The time taken to converge to the unique solution is inversely proportional to T (Fig. 2C). The value $T=0.01$ seconds was chosen here for the specific example switch, CaMKII, whose dissociation constant (k_3) is at least 100-fold smaller than the activation constant (k_2) that governs the rate of autophosphorylation [43]. Unlike the larger value of $T=0.1$ seconds, $T=0.01$ permits quick convergence and reliable encoding for the action potential frequencies characteristic of hippocampal CA3-CA1 synaptic input (approximately 1-15 Hz) [44]. Smaller values of T permit rapid convergence and more sensitive

frequency coding, but may become overly sensitive to temporary lulls in activity when c briefly drops below the leftmost c_c (recall Fig. 1B, i).

It should be noted that $r > 0.65$ is an absolute guarantee of convergence to a unique frequency driven solution; but, from the bifurcation analysis (Fig. 1B, iii; Methods), we know that bistability does not exist for this value. However, in general, only $-r + p(u, x, 2) < 0$ is required, which, for low and high concentrations of activated switch, is obtained at smaller values of r that support bistability. Although a unique encoding of sub-state solutions still exists for smaller r values, convergence about the low activation state is vulnerable to perturbation by short Ca^{2+} inter-pulse intervals, thus acting as a high frequency event (burst) detector through induction of long term switch activation (i.e., hysteresis; Fig. 2D). In theory, this dynamic threshold (the separatrix), is sensitive to recent levels of activation, and could be purposefully modulated by the cell through regulation of the parameters r and c_0, that is, the expression of protein phosphatases and residual levels of cytosolic Ca^{2+} [45]. To restore the low state, the cell simply needs to adjust c_0 to fall below the leftmost critical value c_c. Note, in this simulation, the kernel was specifically chosen to be 30 ms based on literature values for the time course of local synaptic Ca^{2+} signals [15, 46, 47].

Realistically, the Hill function exponent need not be restricted to integer values, which is unlikely in real biological systems. Thus, in the above proof, the expression $p(u, x, n)$ is left as $\frac{u^n - x^n}{(u-x)(1+u^n)(1+x^n)}$ for $n \in \mathbb{R}^+$, since there is no longer a closed form expression for the factorization of the numerator by $u - x$. The function $p(u, x, n)$ has only one critical point at $u = x$, which occurs at an apparent discontinuity due to the factor $u - x$ in the denominator. However, assessing the limit as the difference between x and u becomes infinitesimally small, making the change of variable

$u = x + h$ as $h \to 0$, and recognizing the limit definition of the power rule for differentiation, yields an expression for the maximum of $p(u,x,n)$ $\forall u,x,n \in \mathbb{R}^+$:

$$\begin{aligned}
\max[p(u,x,n)] &= \lim_{u\to x} p(u,x,n) \\
&= \lim_{u\to x}\left[\frac{u^n - x^n}{(u-x)(1+u^n)(1+x^n)}\right] \\
&= \lim_{h\to 0}\left[\frac{(x+h)^n - x^n}{(x+h-x)}\right]\cdot\lim_{h\to 0}\frac{1}{(1+(x+h)^n)(1+x^n)} \\
&= \frac{d}{dx}\left(x^n\right)\cdot\frac{1}{(1+x^n)^2} \\
&= \frac{nx^{n-1}}{(1+x^n)^2}
\end{aligned}$$

For each value of the exponent n, the global maximum of this expression is determined for $\forall x \in \mathbb{R}^+$, and plotted (Fig. 2E). For $n > 0.012$, the minimum of the class of functions $p(u,x,n)$ is found at $n = 1.55$. Fascinatingly, the αCaMKII isoform was reported by De Koninck and Schulman to have a Hill function exponent of 1.6 [11]; although their Hill function argument was Ca^{2+}-CaM, this striking match suggests that αCaMKII's activation function may operate with this particular exponent as it provides the minimum level of negative regulation required to maintain convergence of unique input driven switch activity, even at intermediate levels of the switch response, where r must be stronger to guarantee unique solutions about the low activation state. This has the putative benefit of minimizing the amount of broadly acting phosphatase that may interfere with a cell's other phosphorylation-dependent processing. The reader should note that this result is independent of the model parameters, suggesting it is a very general property of the Hill function and regulated, self-excitatory biological phenomena.

Molecular Switches and Stochastic Resonance

If the model is to capture actual molecular switch behaviour *in vivo*, then we must understand frequency coding in the presence of noise. The results presented in this section are generated by Equation 2 with additive Ornstein-Uhlenbeck noise, $\eta(t)$, which evolves according to the stochastic differential equation

$$\frac{d\eta}{dt} = -\frac{\eta}{\tau_\eta} + \xi(t)$$

where $\xi(t)$ is bounded Gaussian noise, $N(0,1)$, whose amplitude is scaled by a parameter σ. The choice of the time constant τ_n is based on previous studies of noisy microdomain Ca^{2+} fluctuations, where an upper bound for the autocorrelation time was determined to be approximately 10 ms [48, 49]. This choice has the added benefit of matching our switch time constant T, should we instead assume the noise is inherent to switch activation. Figure 3A shows the power spectrum (P_c) of a weak sinusoidal calcium oscillation, $c = c_0 + \alpha \sin(2\pi\varphi t)$, where $c_0 = 0.04$, $\alpha = 0.02$ and $\varphi = 2$ Hz, which was selected based on the mean action potential frequency associated with the CA3 and CA1 regions of the hippocampus [50]. As expected, the noisy switch oscillates at the frequency φ, reflected in its power spectrum (P_x). Given our interest in frequency transfer, it is natural to ask whether noise improves or degrades the switch's frequency coding ability. Very recently, the model of Lewis et al., studied under the context of genetic regulation with $n = 2$, has been shown to produce the stochastic resonance effect [38], which is confirmed here (Fig. 3B). As σ increases from 0, frequency transfer, measured as the ratio of switch power to signal power at φ, dips slightly and then improves dramatically, achieving a maximum at 0.29, followed by a quick decrease as the noise becomes dominant. When changing the exponent from $n = 2$ to $n = 1.6$, this spectral amplification becomes significantly larger, suggesting again that presynaptic αCaMKII functions as a powerful frequency decoder and that the exponent $n =$

1.6 has evolved to optimize this purpose. The reader should note that, for comparisons sake, $r = 0.65$ and $r = 0.61$ were selected respectively for $n = 2$ and $n = 1.6$ based on Fig. 2E, but that this effect is robust to changes in r and φ. Setting $n = 1.6$ also shifts the optimal noise strength to a substantially lower value, 0.09, which has the putative benefit of harnessing stochastic resonance at lower levels of noise that could otherwise be detrimental to different cellular operations.

The results of Kang et al. [38] depend on a full complement of parameters, which begs the question of whether stochastic resonance is a generic feature of the model switch or whether the effect is only significant for a certain range of the parameters. The dimensional reduction of the switch model performed here allows this question to be easily addressed as a function of the parameters c_0, r and n. Figure 3C shows that the parameter r has significant influence over the value of σ that produces optimal spectral amplification and that, for some combinations of c_0, r and n, the stochastic resonance effect disappears completely. The absence or presence of stochastic resonance may prove useful for deducing parameter ranges of molecular switches *in vitro* and *in vivo*. Furthermore, these noise fluctuations drive state transitions and, depending on their intensity (σ), may generate unimodal or bimodal distributions of switch activation (Fig. 3D); this provides another experimentally testable prediction for αCamKII, given that the switch state controls neurotransmitter release probability (Box 1).

Long timescale switch activation

A potential caveat of the bistable switch model is that, even in the autonomous high activation state, the population of phosphorylated units (x) are still subject to the phosphatase activity (r). This places difficult constraints on the cell for long-timescale activation: if c_0 and r are not controlled carefully, the upstate can be lost. The model effectively represents all of the phosphorylated subunits in a

population of CaMKII molecules (each having twelve phosphorylation sites). When one of these dodecamers becomes fully phosphorylated, it effectively becomes impervious to negative regulation by the phosphatases, since any cleaved subunit will immediately be re-phosphorylated by its neighbouring subunits and the enzyme can be shielded by its interactions with downstream targets [19]. Until now, the work presented here has ignored this feature of CaMKII dynamics. Therefore, we introduce a new variable to represent the level of autonomously activated switch that persists after the stimulus has been removed, even when Ca^{2+} levels drop below the leftmost critical value c_c that supports hysteresis (Fig. 1B, i). Inspired by the work of Pinto et al. [31] (Box 1), we assume that the total amount of autonomously activated switch (X) is simply proportional to the average amount of input and thus, the amount of phosphorylated switch $x(t)$ that occurs over the duration of stimulation, Δt :

$$X = \langle \omega x(t) \rangle = \frac{\omega}{\Delta t} \int_0^{\Delta t} x(t) dt \qquad (3)$$

For simplicity, a basal rate of transition to the fully autonomous state, ω, is assumed. Figure 3E shows the amount of autonomously activated switch in response to repeated realizations of Poisson input over a range of frequencies. Note that the amount of autonomously activated switch performs a logarithmic compression of the average frequency over the course of stimulation, while the instantaneous levels of phosphorylated switch track the instantaneous input frequencies throughout (as in Fig. 2A). As a final validation of the model's ability to produce CaMKII-like behaviour, the essence of De Koninck and Schulman's experimental results ([11]; see Fig. 4 within) and the model of Dupont et al. ([12]; Fig. 3E within) are captured qualitatively by Equations 2 and 3 (Fig. 3F). This required setting T on the order of 10^{-1}, which may reflect altered kinetics under the artificial conditions of their experiment, or the need for further refinement of the model presented here. For instance, the proportion ω is expected to grow larger as more of the subunit population becomes phosphorylated and cooperative activation grows stronger [51, 52], leading to an increased likelihood for individual dodecamers to transition to

the fully autonomous state. This is expected to improve the reproduction of De Koninck and Schulman's results by flattening the curves at lower frequencies and steepening them at higher frequencies [11]. Future work should seek to determine $\omega(x)$, with the hopes of identifying reduced representations of strongly nonlinear CaMKII activation.

Discussion

A main goal of this study was to extend the frequency coding idea of De Koninck and Schulman [11] in a generic switch model that captures the qualitative behaviour of CaMKII. The model of Lewis et al. [33], helps to reconcile contradictory perspectives of CaMKII function [11, 31] and suggests dual streams of information transfer that are temporally multiplexed: over short timescales, where the size and duration of the Ca^{2+} pulse is expected to be stable [32], the molecular switch acts as an encoder of instantaneous frequency information and apparently functions to bidirectionally regulate transmitter release probability at synapses through a combination of enzymatic and non-enzymatic activity (Box 1). Over longer timescales, the switch integrates signal intensity, which dictates long term changes in synaptic strength and is dependent on multiple factors such as slow Ca^{2+}-induced Ca^{2+} release (affecting c_0) [24, 53], the size of the Ca^{2+} pulse, its duration and the mean frequency of stimulation. These latter features are expected to adjust the frequency sensitivity of the system by differentially modulating the relative activation of protein phosphatases [45], which influence the threshold for detecting high frequency events, such as bursts of action potentials [54], that could drive up the switch activation state and influence release probability after the input subsides. Furthermore, phosphatases (r) have been treated statically in this study but actually have a high affinity for Ca^{2+} and their dynamics will additionally contribute to frequency tuning and neurotransmitter release [55-57]. Importantly, the work presented here provides some testable predictions for synaptic physiologists: establishing the presence of both bimodal and unimodal synaptic release that depends on αCaMKII and

noise, as well as studying the real-time modulation of release probability at central synapses by αCaMKII in response to natural, aperiodic stimulation patterns (particularly bursting).

Bistable molecular switches are a conserved feature of cell signalling networks and generate combinatorial power in their collective action [58-60]. Much in the way that the leaky-integrate and fire model has been a successful abstraction of neuronal activity, providing a trade-off between performance and a reduced description that facilitates network studies [61, 62], the model of Lewis et al. captures the core essence of molecular switches while remaining amenable to mathematical analysis. The relative simplicity of the model and its application to diverse signalling pathways make it a useful framework for further theoretical and experimental investigations into signalling networks and cellular computation.

References

1. Berridge, M.J., M.D. Bootman, and H.L. Roderick, *Calcium signalling: Dynamics, homeostasis and remodelling.* Nature Reviews Molecular Cell Biology, 2003. **4**(7): p. 517-529.
2. Clapham, D.E., *Calcium signaling.* Cell, 2007. **131**(6): p. 1047-1058.
3. Smedler, E. and P. Uhlen, *Frequency decoding of calcium oscillations.* Biochim Biophys Acta, 2014. **1840**(3): p. 964-9.
4. Wen, Z.X., et al., *A CaMKII/calcineurin switch controls the direction of Ca2+-dependent growth cone guidance.* Neuron, 2004. **43**(6): p. 835-846.
5. Tao, L., et al., *CAMKII and calcineurin regulate the lifespan of Caenorhabditis elegans through the FOXO transcription factor DAF-16.* Elife, 2013. **2**: p. e00518.
6. Lisman, J., H. Schulman, and H. Cline, *The molecular basis of CaMKII function in synaptic and behavioral memory.* Nature Neuroscience Reviews, 2002. **3**: p. 175-190.
7. Thomas, G.M. and R.L. Huganir, *MAPK cascade signalling and synaptic plasticity.* Nature Reviews Neuroscience, 2004. **5**(3): p. 173-183.
8. de Jong, A.P.H. and D. Fioravante, *Translating neuronal activity at the synapse: presynaptic calcium sensors in short-term plasticity.* Frontiers in Cellular Neuroscience, 2014. **8**.
9. O'Leary, T., et al., *Correlations in ion channel expression emerge from homeostatic tuning rules.* Proc Natl Acad Sci U S A, 2013. **110**(28): p. E2645-54.
10. Hunter, T., *A thousand and one protein kinases.* Cell, 1987. **50**(6): p. 823-9.
11. De Koninck, P. and H. Schulman, *Sensitivity of CaM kinase II to the frequency of Ca^{2+} oscillations.* Science, 1998. **279**: p. 227-230.

12. Dupont, G., G. Houart, and P. De Koninck, *Sensitivity of CaM kinase II to the frequency of Ca2+ oscillations: a simple model.* Cell Calcium, 2003. **34**(6): p. 485-97.
13. Graupner, M. and N. Brunel, *STDP in a bistable synapse model based on CaMKII and associated signaling pathways.* Plos Computational Biology, 2007. **3**(11): p. 2299-2323.
14. Zhabotinsky, A.M., *Bistability in the Ca2+/calmodulin-dependent protein kinase-phosphatase system.* Biophysical Journal, 2000. **79**(5): p. 2211-2221.
15. Graupner, M. and N. Brunel, *Calcium-based plasticity model explains sensitivity of synaptic changes to spike pattern, rate, and dendritic location (vol 109, pg 3991, 2012).* Proceedings of the National Academy of Sciences of the United States of America, 2012. **109**(52): p. 21551-21551.
16. Bornholdt, S., *Less is more in modeling large genetic networks.* Science, 2005. **310**(5747): p. 449-+.
17. Kotaleski, J.H. and K.T. Blackwell, *Modelling the molecular mechanisms of synaptic plasticity using systems biology approaches.* Nature Reviews Neuroscience, 2010. **11**(4): p. 239-251.
18. Lisman, J., H. Schulman, and H. Cline, *The molecular basis of CaMKII function in synaptic and behavioural memory.* Nature Reviews Neuroscience, 2002. **3**(3): p. 175-190.
19. Lisman, J., R. Yasuda, and S. Raghavachari, *Mechanisms of CaMKII action in long-term potentiation.* Nature Reviews Neuroscience, 2012. **13**(3): p. 169-182.
20. Ninan, I. and O. Arancio, *Presynaptic CaMKII is necessary for synaptic plasticity in cultured hippocampal neurons.* Neuron, 2004. **42**(1): p. 129-141.
21. Pang, Z.P., et al., *Calmodulin controls synaptic strength via presynaptic activation of calmodulin kinase II.* J Neurosci, 2010. **30**(11): p. 4132-42.
22. Wang, D. and L. Maler, *Differential role of Ca^{2+}/calmodulin-dependent kinases in posttetanic potentiation at input selective glutamatergic pathways.* Proceedings of the National Academy of Sciences of the United States of America, 1998. **95**: p. 7133-7138.
23. Chapman, P.F., et al., *The α-Ca^{2+}/calmodulin kinase II: A bidirectional modulator of presynaptic plasticity.* Neuron, 1995. **14**: p. 591-597.
24. Catterall, W.A. and A.P. Few, *Calcium channel regulation and presynaptic plasticity.* Neuron, 2008. **59**(6): p. 882-901.
25. Saviane, C., et al., *Frequency-dependent shift from paired-pulse facilitation to paired-pulse depression at unitary CA3-CA3 synapses in the rat hippocampus.* Journal of Physiology-London, 2002. **544**(2): p. 469-476.
26. Hinds, H.L., et al., *Essential function of alpha-calcium/calmodulin-dependent protein kinase II in neurotransmitter release at a glutamatergic central synapse.* Proc Natl Acad Sci U S A, 2003. **100**(7): p. 4275-80.
27. Wang, Z.W., *Regulation of Synaptic Transmission by Presynaptic CaMKII and BK Channels.* Molecular Neurobiology, 2008. **38**(2): p. 153-166.
28. Hojjati, M.R., et al., *Kinase activity is not required for alpha CaMKII-dependent presynaptic plasticity at CA3-CA1 synapses.* Nature Neuroscience, 2007. **10**(9): p. 1125-1127.
29. Thanawala, M.S. and W.G. Regehr, *Presynaptic Calcium Influx Controls Neurotransmitter Release in Part by Regulating the Effective Size of the Readily Releasable Pool.* Journal of Neuroscience, 2013. **33**(11): p. 4625-+.
30. Jackman, S.L., et al., *The calcium sensor synaptotagmin 7 is required for synaptic facilitation.* Nature, 2016. **529**(7584): p. 88-+.
31. Pinto, T.M., M.J. Schilstra, and V. Steuber. *The effective calcium/calmodulin concentration determines the sensitivity of CaMKII to the frequency of calcium oscillations*. in *International Conference on Information Processing in Cells and Tissues*. 2012. Springer.
32. Tank, D.W., W.G. Regehr, and K.R. Delaney, *A quantitative analysis of presynaptic calcium dynamics that contribute to short term enhancement.* Journal of Neuroscience, 1995. **15**: p. 7940-7952.
33. Lewis, J., J.M.W. Slack, and L. Wolpert, *Thresholds in Development.* Journal of Theoretical Biology, 1977. **65**(3): p. 579-590.

34. Chin, D. and A.R. Means, *Calmodulin: a prototypical calcium sensor.* Trends in cell biology, 2000. **10**(8): p. 322-328.
35. Smolen, P., D.A. Baxter, and J.H. Byrne, *Frequency selectivity, multistability, and oscillations emerge from models of genetic regulatory systems.* American Journal of Physiology-Cell Physiology, 1998. **274**(2): p. C531-C542.
36. Zheng, X.D., X.Q. Yang, and Y. Tao, *Bistability, Probability Transition Rate and First-Passage Time in an Autoactivating Positive-Feedback Loop.* Plos One, 2011. **6**(3).
37. Heltberg, M., et al., *Noise Induces Hopping between NF-kappa B Entrainment Modes.* Cell Systems, 2016. **3**(6): p. 532-+.
38. Kang, Y.M., et al., *Mean First Passage Time and Stochastic Resonance in a Transcriptional Regulatory System with Non-Gaussian Noise.* Fluctuation and Noise Letters, 2017. **16**(1).
39. Xiong, W. and J.E. Ferrell, *A positive-feedback-based bistable 'memory module' that governs a cell fate decision.* Nature, 2003. **426**(6965): p. 460-465.
40. Oswald, A.M., J.E. Lewis, and L. Maler, *Dynamically interacting processes underlie synaptic plasticity in a feedback pathway.* Journal of Neurophysiology, 2002. **87**: p. 2450-2463.
41. Regehr, W.G., *Short-Term Presynaptic Plasticity.* Cold Spring Harbor Perspectives in Biology, 2012. **4**(7).
42. Edelstein-Keshet, L., *Mathematical models in biology*. 2005: SIAM.
43. Coultrap, S.J. and K.U. Bayer, *CaMKII regulation in information processing and storage.* Trends Neurosci, 2012. **35**(10): p. 607-18.
44. Mizuseki, K., et al., *Activity dynamics and behavioral correlates of CA3 and CA1 hippocampal pyramidal neurons.* Hippocampus, 2012. **22**(8): p. 1659-1680.
45. Li, L., M.I. Stefan, and N. Le Novere, *Calcium Input Frequency, Duration and Amplitude Differentially Modulate the Relative Activation of Calcineurin and CaMKII.* Plos One, 2012. **7**(9).
46. Sabatini, B.L., T.G. Oertner, and K. Svoboda, *The life cycle of Ca2+ ions in dendritic spines.* Neuron, 2002. **33**(3): p. 439-452.
47. Sinha, S.R., L.G. Wu, and P. Saggau, *Presynaptic calcium dynamics and transmitter release evoked by single action potentials at mammalian central synapses.* Biophysical Journal, 1997. **72**(2): p. 637-651.
48. Weinberg, S.H. and G.D. Smith, *The Influence of Ca2+ Buffers on Free [Ca2+] Fluctuations and the Effective Volume of Ca2+ Microdomains.* Biophysical Journal, 2014. **106**(12): p. 2693-2709.
49. von Wegner, F., N. Wieder, and R.H. Fink, *Microdomain calcium fluctuations as a colored noise process.* Front Genet, 2014. **5**: p. 376.
50. Csicsvari, J., et al., *Ensemble patterns of hippocampal CA3-CA1 neurons during sharp wave-associated population events.* Neuron, 2000. **28**(2): p. 585-594.
51. Chao, L.H., et al., *Intersubunit capture of regulatory segments is a component of cooperative CaMKII activation.* Nature Structural & Molecular Biology, 2010. **17**(3): p. 264-U23.
52. Meyer, T., et al., *Calmodulin Trapping by Calcium-Calmodulin Dependent Protein-Kinase.* Science, 1992. **256**(5060): p. 1199-1202.
53. Sharma, G. and S. Vijayaraghavan, *Modulation of presynaptic store calcium induces release of glutamate and postsynaptic firing.* Neuron, 2003. **38**(6): p. 929-939.
54. Krahe, R. and F. Gabbiani, *Burst firing in sensory systems.* Nat Rev Neurosci, 2004. **5**(1): p. 13-23.
55. Klee, C.B., T.H. Crouch, and M.H. Krinks, *Calcineurin - Calcium-Binding and Calmodulin-Binding Protein of the Nervous-System.* Proceedings of the National Academy of Sciences of the United States of America, 1979. **76**(12): p. 6270-6273.
56. Winder, D.G. and J.D. Sweatt, *Roles of serine/threonine phosphatases in hippocampal synaptic plasticity.* Nature Neuroscience Reviews, 2001. **2**: p. 461-474.
57. Sun, T., et al., *The Role of Calcium/Calmodulin-Activated Calcineurin in Rapid and Slow Endocytosis at Central Synapses.* Journal of Neuroscience, 2010. **30**(35): p. 11838-11847.
58. Bhalla, U.S. and R. Iyengar, *Emergent properties of networks of biological signaling pathways.* Science, 1999. **283**(5400): p. 381-387.

59. Ferrell, J.E., *How responses get more switch like as you move dawn a protein kinase cascade.* Trends in Biochemical Sciences, 1997. **22**(8): p. 288-289.
60. Brandman, O., et al., *Interlinked fast and slow positive feedback loops drive reliable cell decisions.* Science, 2005. **310**(5747): p. 496-498.
61. Burkitt, A.N., *A review of the integrate-and-fire neuron model: I. Homogeneous synaptic input.* Biological Cybernetics, 2006. **95**(1): p. 1-19.
62. Jolivet, R., et al., *The quantitative single-neuron modeling competition.* Biological Cybernetics, 2008. **99**(4-5): p. 417-426.
63. Freedman, D. and P. Diaconis, *On the Histogram as a Density Estimator - L2 Theory.* Zeitschrift Fur Wahrscheinlichkeitstheorie Und Verwandte Gebiete, 1981. **57**(4): p. 453-476.

Acknowledgements: I would like to thank Lin Wang for useful discussions and input during the early stages of the project, as well as Leonard Maler and Richard Naud for proofreading the manuscript and providing valuable comments. This work was funded by training grants awarded to S.E.C. from both the National Sciences and Engineering Research Council of Canada and the Canadian Institute of Health Research.

Methods:

Bifurcation Analysis

The first step of the bifurcation analysis is to find the equilibrium points. Setting $n = 2$, we rewrite Equation 1 as,

$$\frac{dx}{dt} = g(x) - h(x)$$

where $g(x) = \frac{x^2}{1+x^2}$ and $h(x) = rx - c$. The fixed points occur when $g(x) - h(x) = 0$, which amounts to finding the solutions of the polynomial $-rx^3 + (c+1)x^2 - rx + c = 0$. First, fix c and examine the effects of varying r. When $c = 0$, $x = 0$ is a fixed point, and, for a particular range of r, there exists two

other positive valued fixed points, given by the roots of $-rx^2 + x - r = 0$. The critical value of the parameter r, denoted by r_c is found by setting $g(x) = h(x)$ and $g'(x) = h'(x)$, which, when solved, gives $r_c = \frac{x}{1+x^2} = \frac{2x}{(1+x^2)^2}$. Three values of x satisfy this equality: -1, 0 and 1. Since we are not considering negative values of x, we have two critical points, $r_c = 0$ and $r_c = \frac{1}{2}$. Therefore, when $c = 0$, the system is bistable for $0 < r < \frac{1}{2}$. For $c > 0$, r can be larger than $\frac{1}{2}$ while still preserving bistability (as in Fig. 1A). We know r_c occurs when $h(x) = g(x)$ and $h'(x) = g'(x)$; therefore, when $h(x) > g(x)$ we lose a fixed point through a saddle node bifurcation. For $x > 0$, the maximum of $g(x)$ is found at $x = \sqrt{\frac{1}{3}}$ which gives $\max_x[g(x)] = \frac{3\sqrt{3}}{8}$. Therefore, when $r > r_c = \frac{3\sqrt{3}}{8}$, only one fixed point exists.

Now, we are interested in fixing r and examining the effects of varying c. To find c_c we set $g(x) = h(x)$ and $g'(x) = h'(x)$, which gives $r = \frac{2x}{(1+x^2)^2}$ and $c_c = rx - \frac{x^2}{1+x^2}$. Substituting the first expression into the second, we get $c_c = \frac{x^2(1-x^2)}{(1+x^2)^2}$. We differentiate with respect to x in order to locate the maximum value for c_c; $0 = \frac{2x(1-3x^2)}{(1+x^2)^3}$. This gives $x = 0$ and $x = \sqrt{\frac{1}{3}}$, which corresponds to $c_c = 0$ and $c_c = \frac{1}{8}$. When $c > c_c$, only one fixed point exists for all values of r. For a fixed value of r that supports bistability, as c increases from 0 and crosses a critical value (c_c), the fixed point x^* will jump up to the high amplitude branch. If c is now decreased, the fixed point remains on the high amplitude branch even as c becomes smaller than the corresponding c_c. This hysteresis effect permits

switch activation to remain as the transient Ca^{2+} signal subsides, consistent with the findings from synaptic plasticity experiments (Box 1). Using the expressions derived for the critical values of r_c and c_c, we plot them parametrically as functions of x (Fig. 1B, iii). Saddle node bifurcations occur all along the boundary of these curves, it is here we find the values of r and c for which only two fixed points occur. Crossing each branch results in a pairwise collision and disappearance of two fixed points. Note where the bifurcation curves meet tangentially, $(c,r) \to \left(\frac{1}{8}, \frac{3\sqrt{3}}{8}\right)$, here we observe a co-dimension two bifurcation; beyond this point there is only one fixed point and the distinction between low and high activation states is blurred (Fig. 1B, iii).

Computational Specifications and Miscellaneous Details

Simulations were solved using the 4th order Runge-Kutta method, with the exception of the Ornstein-Uhlenbeck noise, which was solved using the stochastic Euler method (time step of 1 ms in all cases). All simulations were performed using custom code, available upon request to the author, and were implemented on a Linux machine running Ubuntu 16.04 with an Intel core i7-6700 CPU, 3.4 GHz processing speed, and 62 GB of RAM.

Pulse train sequences $\{t_i\}$ were convolved with the filter $t \cdot e^{-(t-t_i)/\tau_c}$, whose decay constant τ_c was set to 30 ms, reflecting an accommodation of both pre- and post-synaptic calcium decay values from the literature that range from 15-43 ms [15, 46, 47]. The resulting input signal was normalized to the maximum value and then scaled by Δc .The decay value is closely related to the input frequencies typical of a given synapse and the definition of what constitutes a high frequency event in the system, since for events occurring faster than the decay, Ca^{2+} accumulates quickly, driving the switch into the

upstate. The putative burst detector will work for different τ_c, but may require a different set of corresponding switch parameters, range of stimulation frequencies and pulse amplitudes.

Histogram bin sizes for Fig. 3D were set using the Freedman-Diaconis method [63].

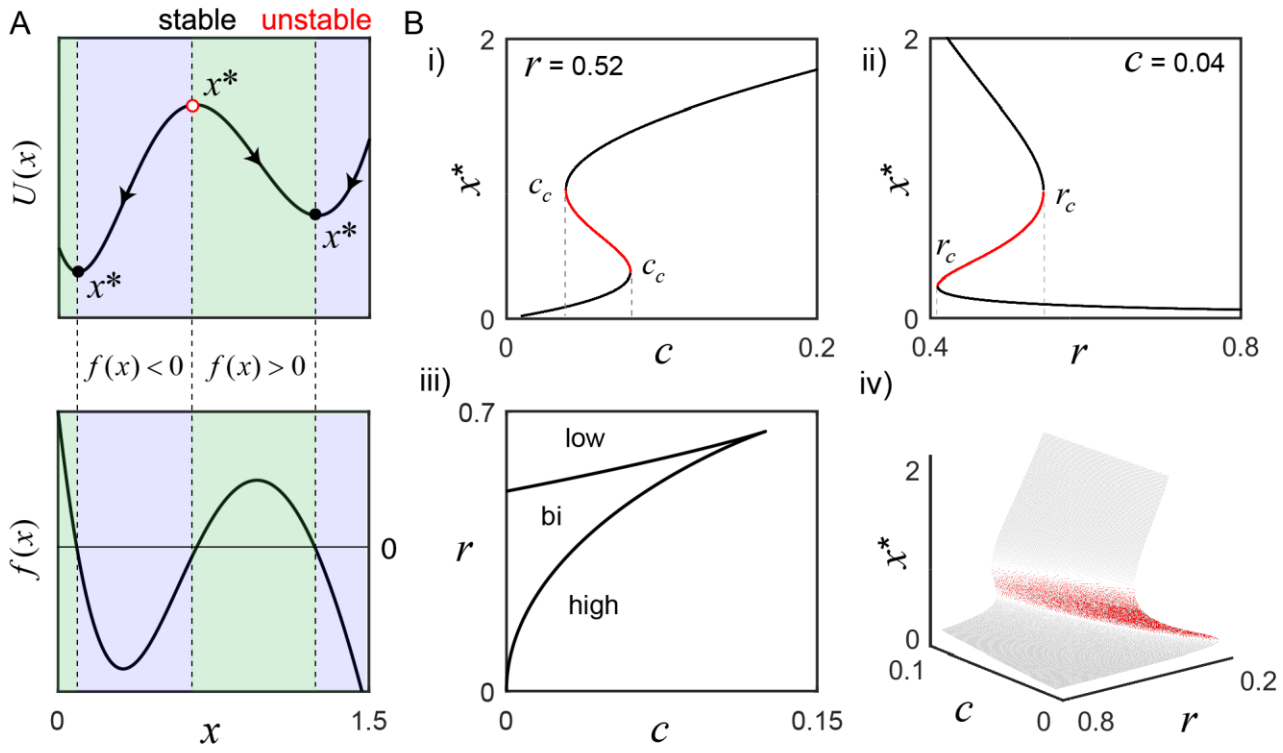

Figure 1 **Activation states of the bistable molecular switch model** **A)** The model's potential function, $U(x)$, visually describes the tendency for solutions to settle around one of two equilibrium points (x^*), where the rate of change of switch activation, $f(x)$, is 0 (parameters, $r = 0.52$ and $c = 0.04$). To the left of the stable equilibria (black circles), $f(x) > 0$ (green), and to the right, $f(x) < 0$ (blue), forcing perturbations to settle back into those states. Conversely, the sign of $f(x)$ is reversed on both sides of the unstable equilibrium (red circle), such that tiny perturbations push the switch away, toward either stable state. **B)** As r or c change, $f(x)$ changes and can result in the loss of bistability. **(i)** To illustrate, r is fixed as the input c is varied: small values only support low activation, but, as c grows, bistability emerges and eventually only the high activation state is supported when $c > c_c$ (rightmost). A defining feature of bistability is the hysteresis effect, where the same value of a parameter may evoke different states depending on the history of activity. For example, the high activation state still exists for c less than the rightmost c_c and can only be lost when c falls below the leftmost c_c value. **(ii)** c is fixed while the negative regulation parameter r is varied. For small r, only the high activation state exists. As r grows larger, the system becomes bistable and, eventually, only the low state exists after crossing r_c. Panel **(iii)** shows a parametric plot of the critical values $c_c(x)$ and $r_c(x)$, and the bifurcation surface summarize the analysis completely **(iv)**.

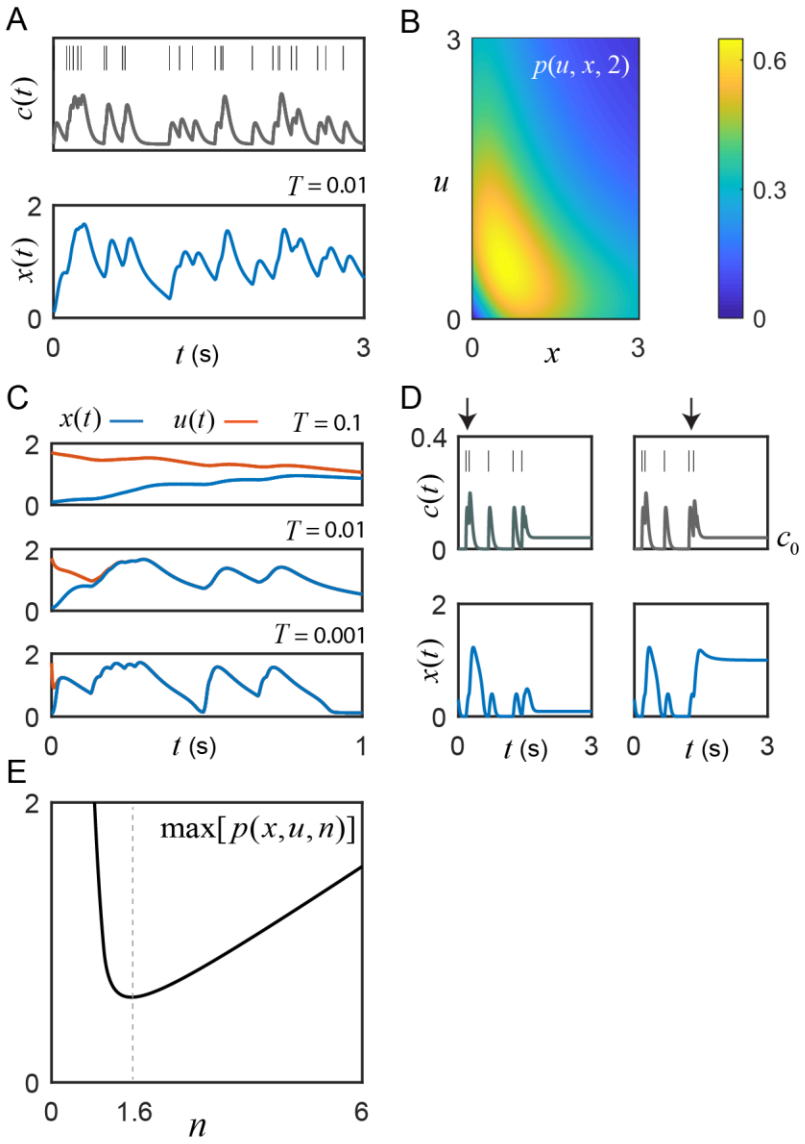

Figure 2 **Switch activity fluctuates with instantaneous input frequency** **A)** Motivating example: switch response to an 8 Hz Poisson sequence of input pulses, convolved with an alpha function kernel to create a signal, $c(t) = c_0 + c_I(t)$. The switch tracks changes in the input frequency ($n = 1.6$, $r = 0.61$, $c_0 = 0.04$, and $T = 0.01$) **B)** The example function $p(u,x,2)$ from the uniqueness proof achieves a maximum of 0.65; r must exceed this critical value to guarantee absolute convergence of the switch to a unique frequency-driven solution. **C)** Initial conditions: $u(0) = 1.7$ and $x(0) = 0.1$. The value of T affects time-to-convergence between solutions and frequency filtering. From empirical studies, $T \le 0.01$ [43]. **D)** For $r < r_c$, sufficiently high frequency event intervals (bursts) cause transitions from the low to high state (illustrated for $n = 2$). By adjusting c_0 to take advantage of hysteresis, the cell can control whether or not it is sensitive to these burst-induced up states. The arrows highlight this fact for c_0 equal to 0 and 0.04; neither static value can generate the upstate alone (Fig. 1B). **E)** In general, the exponent $n \neq 2$ in real biological systems. Interestingly, $n = 1.55$ is a minimum for the maximum value of the class of functions $p(u,x,n)$ in the uniqueness

proof, that is, the value of r needed to guarantee convergence of solutions in self-exciting bistable systems. This is remarkably close to the empirical value of 1.6 reported by De Koninck and Schulman for presynaptic αCaMKII [11].

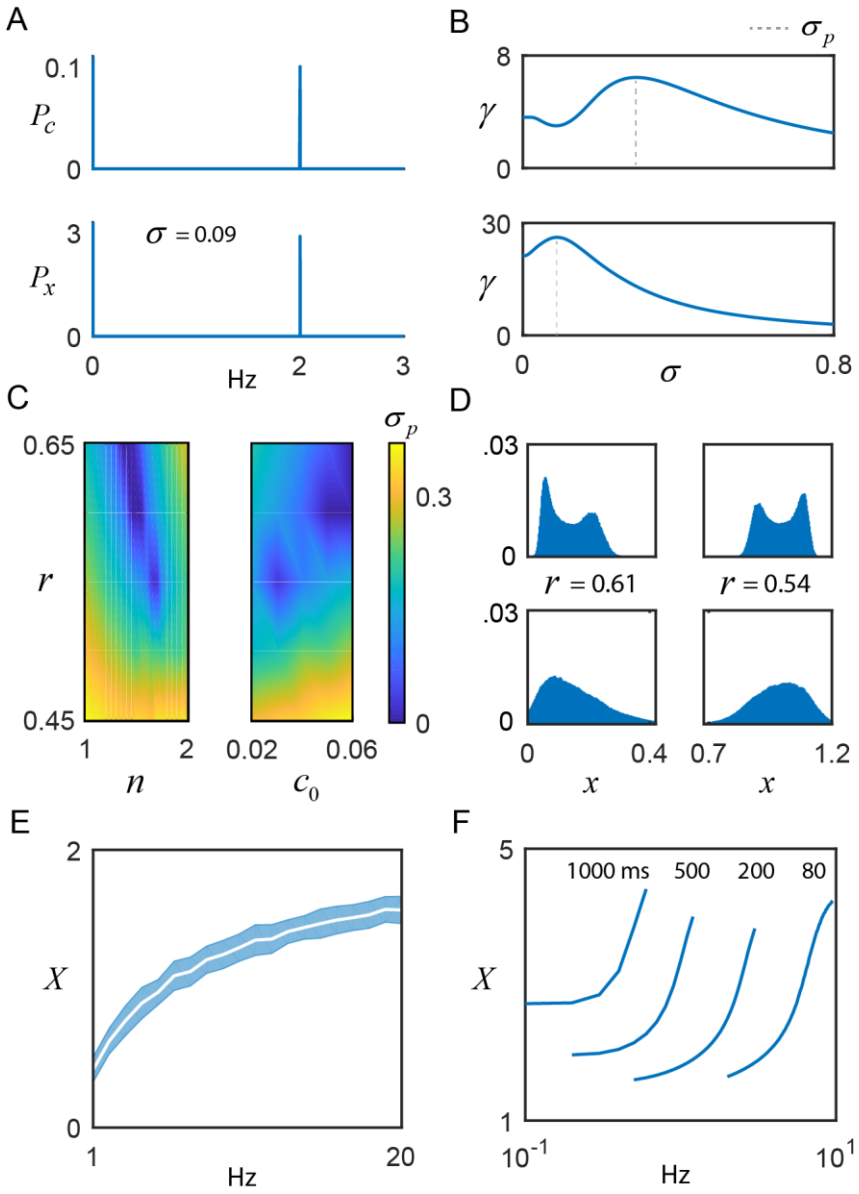

Figure 3 **Frequency coding with noisy switches** **A)** The switch model driven by a weak sinusoidal signal, $c(t) = c_0 + \alpha \sin(2\pi\varphi t)$, with $c_0 = 0.04$, $\alpha = 0.02$, $\varphi = 2$ Hz, and additive noise, $\eta(t)$, whose intensity is scaled by the parameter σ and evolves according to $\tau_\eta = 0.01$. The switch amplifies the frequency content of the input, as shown by its power spectrum P_x relative to the signal's, P_c. **B)** *Top*: For $n = 2$, the ratio of switch power to signal power at φ is plotted as a function of the noise intensity σ, achieving a maximum at 0.29, that is, the switch displays stochastic resonance (SR). The value of σ that promotes optimal frequency transfer is denoted by σ_p. *Bottom*: For $n = 1.6$, there is substantially larger gain in the SR effect, and σ_p shifts to 0.09. **C)** σ_p is plotted as a function of (n, r) and (c_0, r), illustrating the presence or absence of SR. **D)** For $n = 1.6$, noisy switch activity produces bimodal (e.g., $\sigma = 0.01$) or unimodal (e.g., $\sigma = 0.035$) states of activation, which is likely reflected in synaptic release probability (Box 1); the relative occupation of the high state versus the low state depends on r. **E)** The activated switch, X, driven by multiple realizations of Poisson input,

logarithmically compresses the mean input frequency (shading: +/- standard deviation), while instantaneous switch activity tracks the instantaneous input frequencies. **F)** As a model validation, the pulse duration (in ms) and frequency experiments of De Koninck and Schulman were simulated ($n = 1.6$, $r = 0.61$ and $T = 0.4$), qualitatively capturing their results.